Taylor & Francis
Taylor & Francis Group

Computational Studies of Lead-based Relaxor Ferroelectrics

HIROYUKI TAKENAKA,[1] ILYA GRINBERG,[1]
YOUNG-HAN SHIN,[2] AND ANDREW M. RAPPE[1]

[1]The Makineni Theoretical Laboratories, Department of Chemistry, University
of Pennsylvania, Philadelphia, PA 19104-6323
[2]Department of Physics, University of Ulsan, Ulsan 680-749, Korea

Relaxor ferroelectrics have been a focus of intense attention due to their fascinating physical properties. Their diffuse phase transitions have been explained by the polar nanoregion model. Nevertheless, fundamental characterization of structure and dynamics in relaxors is still a long-standing challenge. Better scientific understanding of the microscopic origins of relaxor behavior is also required to improve efficiencies of relaxor based devices. Our molecular dynamics studies in 0.75PbMg$_{1/3}$Nb$_{2/3}$O$_3$-0.25PbTiO$_3$ showed good agreement with experimental data and revealed conflicts with the current polar nanoregion model. Here, we review our work and propose an alternate model for structure and dynamics in the relaxor phase.

Keywords Relaxor ferroelectrics; dielectric dispersion; dipole relaxation time; dynamics

1. Introduction

A relaxor ferroelectric material was first synthesized by Smolenskii *et al.* in 1961 [1]. Relaxors are mainly lead-based perovskite solid solutions and exhibit a stronger piezoelectric effect, high permittivity over a broad temperature range, unique dielectric response with strong frequency dispersion, and anomalous phonon dispersion relations [2–7]. Relaxors are used in transducers and capacitors due to the excellent dielectric and piezoelectric properties. For example, prototypical $(1 - x)$Pb(Mg$_{1/3}$,Nb$_{2/3}$)O$_3$-xPbTiO$_3$(PMN-PT) relaxors form the core of the state-of-the-art ultrasound medical imaging probes. However, in SONAR transducers, conventional crystalline Pb(Zr,Ti)O$_3$ (PZT) is widely used despite the fact that relaxors show about four to ten times larger the d_{33} coefficients. This is due to loss of piezoelectric performance below unsuitably low Curie temperature and low coercive fields in the relaxors compared with PZT. Currently, experimental and theoretical investigations of relaxors are ongoing due to the technological applications and scientific interest of these materials.

Color versions of one or more of the figures in the article can be found online at www.tandfonline.com/gfer.

The diffusive and dispersive characteristics of the inverse dielectric response are signatures of relaxor behavior. The diffuse phase transitions that take place gradually are called relaxed phase transitions, giving rise to the term *"relaxor"*. In 1983, Burns and Dacol found that the inverse of dielectric response starts deviating from the Curie-Weiss law at the Burns temperature (T_b) [8,9] that is significantly above the Curie temperature (T_c) in $Pb(Mg_{1/3}Nb_{2/3})O_3$ (PMN). They ascribed this to the appearance of polar nanoregions (PNR). In the widely accepted current PNR model, the size and the interactions of the PNRs increase inside a non-polar matrix as T is lowered until the growth and the dynamics of the PNRs freeze in at the Vogel-Fulcher freezing temperature (T_f). The origin of these fascinating physical properties has been assigned to local random fields arising from charge-disordered cation arrangement, similar to the smeared out transitions found in spin glass models [10–12]. In the mid 1990s, the X-ray diffraction diffuse scattering and neutron scattering pair distribution functions (PDFs) showed some evidence of the PNRs in the relaxor phase [13,14]. Several investigations also demonstrated the appearance of static polarization above T_c and its influence on on dynamics in relaxors. Using NMR experiments, Blinc *et al.* showed that a local Edwards-Anderson spin glass order parameter appears at a temperature T^* roughly halfway between T_b and T_f [15] and explained the order parameter temperature dependence using the spherical random-bond-random field model [16]. Since then Raman, NMR, neutron scattering pair distribution function (PDF), and diffuse scattering techniques [17–20] have been used to study the structure and dynamics of relaxors and have all showed the presence of the T^* transition temperature. Nevertheless, the definition of a local order parameter to describe the transition from the paraelectric phase to the relaxor phase at T_b is still lacking.

In the present paper, we review our several recent studies of relaxors using first-principles-based modeling. Section 2 presents predictions of relaxor-to-ferroelectric compositional phase transition of lead based perovskite systems by simple Landau theory with two parameters using average structure features calculated by density functional theory. This indicates the relationship between local structures and relaxor dielectric response [21]. In Section 3, we show that the nucleation sites for the relaxor behavior are attributed to a high concentration of neighboring Ti atoms. The dielectric response in the 1080-atom 0.75PMN-0.25PT supercell exhibit frequency dispersion and deviation from the Curie-Weiss law despite the fact that PNR cannot exist in such a small supercell [22]. In Section 4, we review our work on the characterization of local order parameters with instantaneous and time averaged pair distribution functions. We show that highly anisotropic in-phase motion correlations for cation-cation atomic pairs are present in 0.75PMN-0.25PT; these are contradictory to the widely accepted PNR model and are analogous to the hydrogen bond network in water [23]. We therefore suggest a new model of relaxor behavior replace the current PNR/matrix-based model. Our conclusions are presented in Section 5.

2. Landau Theory of Relaxor Behavior in Lead Based Perovskite

Following the work of Setter and Cross, charge-disordered cation arrangement has been assigned as the origin of relaxor behavior [24]. Many relaxor compounds including ternary systems have been discovered. To guide the synthesis of new relaxor materials, we seek a relationship between the cation arrangement and relaxor behavior. As the starting point, we focus on the influence of off-center cation displacements and local cation disorder on the dielectric dispersion that is the defining feature of relaxor materials.
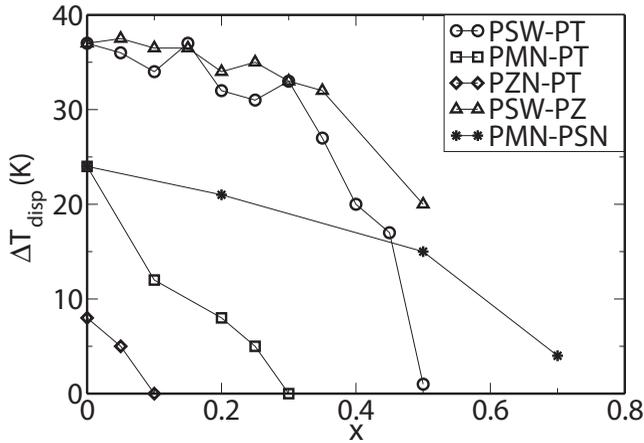
Figure 1. The experimentally measured ΔT_{disp} for the $(1-x)$PSW-xPT, $(1-x)$PMN-xPT, $(1-x)$PZN-xPT, $(1-x)$PSW-xPZ, and $(1-x)$PMN-xPSN solid solutions from Prediction of Dielectric Dispersion for Lead-Based Perovskites and Study of Local Dielectric Response in 0.75Pb(Mg$_{1/3}$Nb$_{2/3}$)O$_3$ -0.25PbTiO$_3$, Ilya Grinberg et al., *Journal of Advanced Dielectrics*, Vol. 2, Issue No. 2, Copyright @ 2012 World Scientific Publishing Company. The dependence of ΔT_{disp} on composition is different for the different relaxor solid solutions.

To quantify the strength of dielectric dispersion, we define ΔT_{disp} as

$$\Delta T_{\text{disp}} = T_{\epsilon,\text{max}}(10^2 \text{Hz}) - T_{\epsilon,\text{max}}(10^6 \text{Hz}) \tag{1}$$

where $T_{\epsilon,\text{max}}$ (10^2 Hz) and $T_{\epsilon,\text{max}}(10^6$ Hz) are the temperatures at the peak heights of the dielectric response for $\omega = 100$ Hz and $\omega = 1$ MHz, respectively. Figure 1 shows that experimental ΔT_{disp} data for the PMN-PT, PMN-Pb(Sc$_{1/2}$Nb$_{1/2}$O$_3$ (PMN-PSN), $(1-x)$Pb(Sc$_{2/3}$W$_{1/3}$)O$_3$-xPbTiO$_3$ (PSW-PT), $(1-x)$Pb(Sc$_{2/3}$W$_{1/3}$)O$_3$-xPbZrO$_3$ (PSW-PZ) and $(1-x)$Pb(Zn$_{1/3}$Nb$_{2/3}$)O$_3$-xPbTiO$_3$ (PZN-PT) solid solutions describe the compositional phase transitions between relaxor and ferroelectric phases in these materials. We therefore assign ΔT_{disp} as an order parameter for the compositional relaxor-to-ferroelectric phase transitions.

Two key variables describe how compositional changes affect ΔT_{disp}. The first one is the cation arrangement on the B-site. PbSc$_{1/2}$Ta$_{1/2}$O$_3$ (PST) exhibits $\Delta T_{\text{disp}} > 0$ for disordered B-site arrangement, while PST with a rocksalt Sc/Ta arrangement [24] exhibits FE behavior. Similarly, Juhás and Davies reported that B-cation disordered arrangement increases the dispersion in PSW-PT solid solutions [25]. A disordered B-cation arrangement in lead-based relaxors leads to the presence of under- and over-bonded oxygen atoms [26], suggesting that overbonded and underbonded oxygen atoms play a key role in the relaxor dispersion. We therefore use the second moment of the B-cation valence of an oxygen atom ($\langle V^2 \rangle$) to be a local structural parameter to characterize the magnitude of variation in the local structure. This is defined as

$$\langle V^2 \rangle = \frac{1}{N_{\text{O}}} \sum_i \left(V_{i,1}^B + V_{i,2}^B - 2\overline{V^B} \right)^2, \tag{2}$$

where $V_{i,1}^B$ and $V_{i,2}^B$ are the valences of the two nearest B-cation neighbors of an O atom, and $\overline{V^B}$, equal to eight in this work, is the averaged valence sum of the two neighbor B-cations in Pb-based perovskites.

The other key variable is the average displacement (D_{avg}^B) of the B-cations in the material as obtained by DFT calculations. The computational details of the DFT calculations are given in Refs. [21] and [27]. The influence of D_{avg}^B on dispersion can be seen from the comparison of ΔT_{disp} values of PZN and PMN as shown in Figure 1. The magnitude of ΔT_{disp} for PZN is about three times smaller than that for PMN. Although the formal charges of the Zn and Mg cations are identical and their ionic radii are almost the same, DFT calculations reveal that the average displacement magnitude of Zn ions in PZN is 0.14 Å and that of Mg ions in PMN is 0.05 Å [27]. This suggests that the average B-cation displacement and ΔT_{disp} are related. Another indication of this relationship can be seen in Samara's study of relaxor dispersion at different pressures in La-doped PZT [28]. The pressure dependent ΔT_{disp} varies linearly from 6 K at ambient pressure to 18 K at a pressure of 20 kbar showing the similar trend as the comparison between PZN and PMN. Thus, the smaller volume due to high pressure increases the ΔT_{disp}. A smaller volume also induces a smaller D_{avg}^B, as has been shown by DFT calculations [29]. Therefore, the changes of ΔT_{disp} observed by Samara agree with the correlation between lower D_{avg}^B and higher ΔT_{disp}.

To predict ΔT_{disp} with the $\langle V^2 \rangle$ and D_{avg}^B, we first propose a simple linear relationship

$$\Delta T_{\mathrm{disp}} = a_{\mathrm{v}} \langle V^2 \rangle + a_D D_{\mathrm{avg}}^B + C, \tag{3}$$

where a_{v}, a_D, and C are constants, fitted with experimental ΔT_{disp}, obtain in Ref. [21]. We also found a similarity between the behavior of ΔT_{disp} as a function of $\langle V^2 \rangle$ and the dependence of the order parameter on temperature in standard Landau theory of a second-order phase transition. Therefore, combining the $\langle V^2 \rangle$ and D_{avg}^B, we define a Landau theory equation for the compositional ferroelectric-to-relaxor phase transition with the order parameter ΔT_{disp}, as follows,

$$G = G_0 - \frac{1}{2} A\big(\langle V^2 \rangle, D_{\mathrm{avg}}^B\big) \Delta T_{\mathrm{disp}}^2 + \frac{1}{4} \Delta T_{\mathrm{disp}}^4 \tag{4}$$

$$\Delta T_{\mathrm{disp,equil}}^2 = A\big(\langle V^2 \rangle, D_{\mathrm{avg}}^B\big) \tag{5}$$

$$A\big(\langle V^2 \rangle, D_{\mathrm{avg}}^B\big) = a_0 + a_v \langle V^2 \rangle + a_d e^{-\kappa D_{\mathrm{avg}}^B} \tag{6}$$

where G is the free energy of the relaxor phase, G_0 is the energy of the parent ferroelectric phase and the Landau coefficient A is a function of $\langle V^2 \rangle$ and D_{avg}^B (a_0, a_v, a_d and κ are constants). We treat the dependence of $A(\langle V^2 \rangle, D_{\mathrm{avg}}^B)$ on D_{avg}^B as the exponential form. The comparison of the experimental ΔT_{disp} values and those predicted by the fits are presented in Figure 2 for lead-based relaxors with various compositions (see Ref. [21] for details). Both show good agreement, but the Landau theory based ΔT_{disp} have smaller errors compared with the linear relationship in Eq. (3). The good agreement between predicted and experimental ΔT_{disp} indicates that local structure in nano-scale order controls the dielectric dispersion in the relaxor materials.
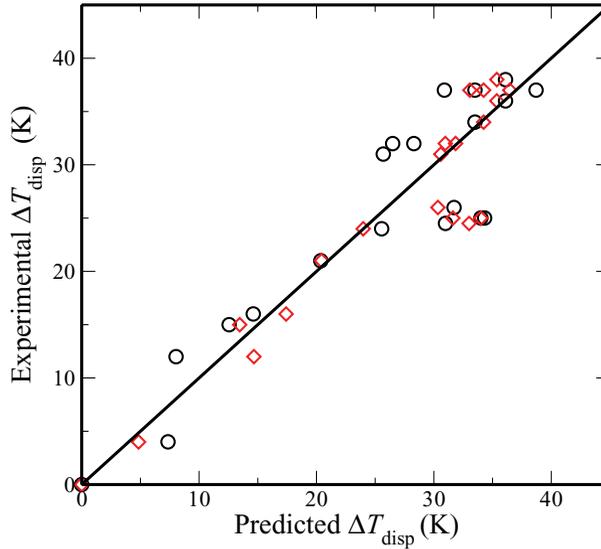
Figure 2. Experimental ΔT_{disp} vs. computationally predicted ΔT_{disp}. The data are taken from [21]. Red circles are fitted values using linear model in Eq. 3 and black diamonds represent the values fitted by the Landau theory model in Eq. 4. The plots show almost linear behavior indicating that both models can reproduce the ΔT_{disp} well with the parameters obtained from DFT calculations.

3. The Role of *B*-cation Environment in the Dielectric Response of a Relaxor Ferroelectric

The concept of the PNR was first suggested to explain the deviation from the Curie-Weiss law at T_b and the other aspects of relaxor behavior by Burns [8,9] and now has been widely accepted. However, our MD simulations with a nano-scale 1080-atom supercell reproduce the frequency dispersion and deviation from the Curie-Weiss law. Such a supercell is too small to include PNR and a non-polar matrix.

We performed the first-principles based bond valence molecular dynamics (BVMD) simulations for study of relaxation lifetimes of the individual unit cell dipole moments in the 0.75PMN-0.25PT material using small $6 \times 6 \times 6$ supercells with ≈ 1.5 ns simulation time. Computational details are given in Ref. [22]. We used the random site rock-salt arrangement model [30] to generate the *B*-cation arrangement; the randomness on one of the cation sublattices produces over- and under-bonded oxygen atoms which give rise to dielectric dispersion in lead-based relaxors.

We examine the relaxation lifetimes of the dipoles for individual *B*-cation sites to analyze the roles of the *B*-cations in the dielectric response. The relaxation lifetimes are estimated by the autocorrelation functions of dipole moments obtained from MD simulations. The different *B*-cation sites are classified based on their local *B*-cation environment. For Mg and Ti atoms, *B*-cations in nearest neighbor cells are always Nb atoms. In the case of Nb atoms there are four different groups, due to random occupation of the neighboring *B* sites by Mg and Ti. We label all Nb atoms as $\text{Nb}^{C'C''}$; where C=M or T stands for Mg or Ti, respectively and C' is a neighbor *B*-cation to the left and C'' is a neighbor *B*-cation to the right. Therefore, we have a total of six different sites, Mg, Nb^{MM}, Nb^{TT}, Nb^{MT}, Nb^{TM}, and Ti respectively. The site relaxation lifetimes sorted into these six groups are plotted in Figure 3.
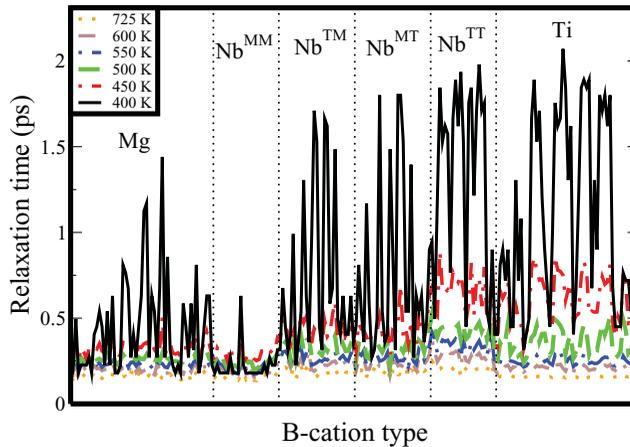
Figure 3. Temperature dependence of unit cell dipole moment relaxation lifetimes τ_i grouped by local environment from [22]. The MD simulation results for 0.75PMN-0.25PT show a clear jump in the τ_i magnitudes below T_b except for the Nb^{MM} cells. This is a signature of the slow dynamics of the relaxor phase.

Above 550 K, the short lifetimes with slightly larger magnitudes for the Nb^{TT} means the system is in the paraelectric phase. At $T = 500$ K, the lifetimes are increased for some Ti sites and are remarkably increased for the Nb^{TT} sites compared with Nb^{MT} and Nb^{TM}. This provides clear evidence for the phase transition and slower dynamics just below the paraelectric-to-relaxor phase transition at T_b. Interestingly, at 400 K, in close proximity to $T_f = 375$ K, although most of the sites exhibit large relaxation lifetimes characteristic of the relaxor phase, the relaxation lifetimes of the Nb^{MM} sites remain at low paraelectric phase values. Thus, we find the Nb atoms with a high concentration of neighboring Ti atoms act as the nucleation sites for the relaxor behavior. This indicates that the higher coupling between the cation displacements arises from the presence of overbonded oxygens.

4. Pair Distribution Functions Study for Local Structure and Dynamics in a Relaxor Ferroelectric

For a locally inhomogeneous system such as a perovskite alloy, real space methods such as PDF analysis are a natural tool for interpretations of the structural effects of the local compositional inhomogeneity that gives rise to the relaxor behavior. Recently, the development of new neutron sources has made dynamic pair distribution function (DPDF) information available from inelastic neutron scattering experiments [19]. This technique provides information about frequencies of vibrations at given interatomic distances.

The PDF analysis of the microscopic details of the structure and dynamics of the different relaxor phases shows that relaxor transitions can be characterized by local order parameters and highly anisotropic correlations of in-phase motions that arise from structural features contradicting the current model of PNR in a non-polar matrix. An alternate model emerges from the interpretations of the correlations.

4.1 Methodology

We study an 8640-atom supercell of 0.75PMN-0.25PT with BVMD simulations and PDF analysis to examine the changes in local structure and dynamics through the relaxor phase transitions. To analyze MD simulation results, we first calculate the $g(r,t)$ generalized pair-distribution function which is the summation of the probability of a distance r of an atomic pair with time delay t defined as $t = t' - t''$, one atom at time t' and the other atom at time t''. The $g(r, t)$ is calculated by means of the correlation function of structure factors at a given distance r and time delay t as follows,

$$g(r, t) = \frac{1}{N\langle b\rangle^2} \sum_{v,\mu=1}^{N} \frac{1}{\sqrt{\pi\sigma_v + \sigma_\mu}} b_v b_\mu \frac{1}{4\pi r^2}$$
$$\times \int e^{-\frac{(r-|R_v(t')-R_\mu(t+t')|)^2}{\sigma_v+\sigma_\mu}} dt' \tag{7}$$

where N is the number of atoms, b is neutron scattering length, $\langle b\rangle$ is the average of the scattering lengths, σ is the normalization factor of the Gaussian smearing width, and R is an atomic position. High peaks of $g(r, t)$ appear at favorable distances and time delays that coincide with the integer multiple of time periods of motions of atomic pairs.

We then Fourier transform the $g(r, t)$ to obtain $G(r, \omega)$ which represents the frequency spectra of the $g(r, t)$ and corresponds to the DPDF intensities obtained by inelastic neutron scattering experiments. It is clear that we can decompose $g(r, t)$ in Eq. (7) into $g_{AB}(r, t)$ defined as the probability of an atom of species A located at distance r from the position of an atom of species B with time delay t and $G(r, \omega)$ into $G_{AB}(r, \omega)$ as well. This enables us to resolve the vibrational frequencies for the different types of atomic pairs at different distances. This is highly advantageous for the analysis of local and compositionally inhomogeneous systems such as relaxors. For structure and dynamics analysis, we also examine $g_{AB}(r,t=0)$, the instantaneous PDF, and $G_{AB}(r,\omega=0)$, the time averaged PDF (see in Ref. [31] for details).

4.2. Results and Discussions

4.2.1 Frequency Averaged DPDF. We first compare our results with the neutron scattering DPDF data of Dmowski *et al.* for pure PMN [19]. As in the experimental work, we extract the phase transition temperatures of our system by examination of the integrated DPDF intensity ($G(r, \omega)$) from 10 meV to 20 meV and from 0 meV to 5 meV for $2 < r < 5$ Å as shown in Figures 4a and 4b, respectively. We also present 1D plots of the integrated DPDF intensities as a function of T to locate the phase transition temperatures through the changes in the temperature dependence of the DPDF intensities at 2.38 Å (Figure 4a), 3.3 Å and 2.58 Å (Figure 4b). The 1D plot of Figure 4a at 2.38 Å (Figure 4c) shows a discontinuity at 550 K in agreement with the experimental Tb = 550 K of 0.75PMN-215 0.25PT [32]. Examination of the 1D plot for the integrated DPDF intensities from 0 to 5 meV at $r = 3.3$ Å in Figure 4d shows that there are two changes at 550 K and at 425 K. The transition at 425 K is close to the intermediate temperature T^* of 0.75PMN-0.25PT [33]. As shown in Figure 4b, the integrated low-frequency DPDF from 0 to 5 meV for $r < 2.8$ Å has a split peak similar to the split peak for the PMN. In Figure 4e, the integrated lower frequency DPDF intensity at $r = 2.58$ Å shows that the intensity starts decreasing at 525 K
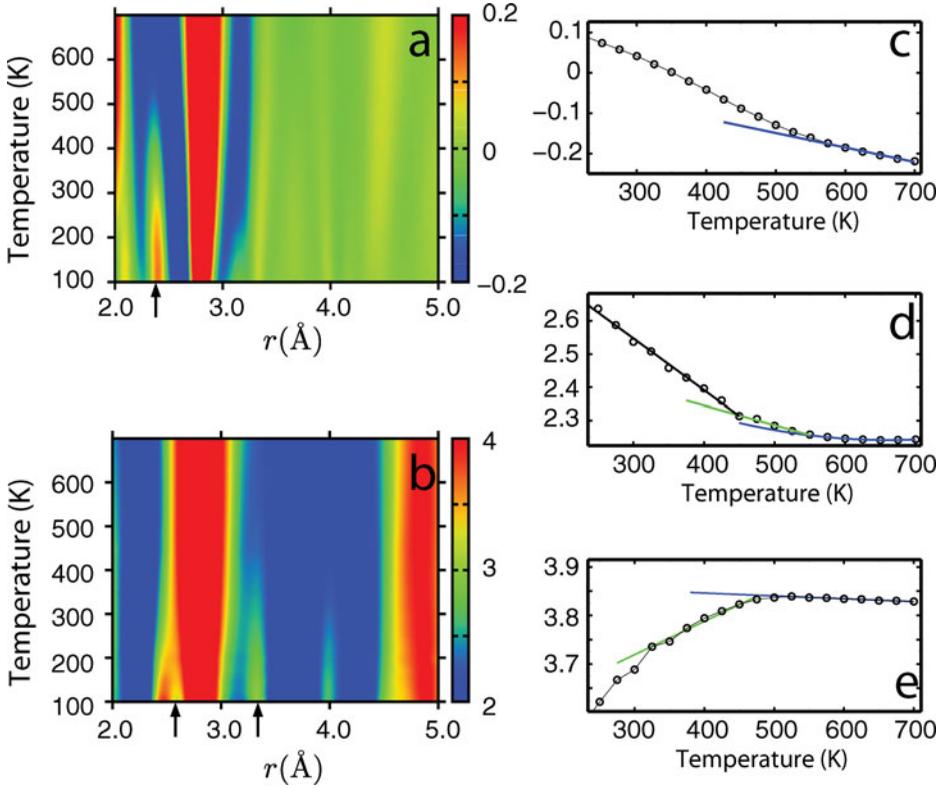
Figure 4. The frequency averaged DPDF. Color contour plot of computational 0.75PMN-0.25PT $G(r, \omega)$ integrated from 10 to 20 meV in (a) and from 0 to 5 meV in (b). The integrated values are given in the color bars multiplied by a factor of 10^4. (c) 1D plot of integrated $G(r, \omega)$ for the high frequency range as a function of T at $r = 2.38$ Å extracted from (a) at a tick. The 1D plots for the lower frequency range at $r = 3.3$ Å in (d) and at $r = 2.58$ Å in (e) from (b) where ticks point out the r values. The data are taken from [23].

and the slope changes at 350 K, slightly below the experimental $T_f = 380$ K of 0.75PMN-0.25PT [32]. The phase transition temperatures for the computational 0.75PMN-0.25PT results agree with the experimentally obtained 0.75PMN-0.25PT temperatures, suggesting that our MD simulations reproduce the structure and dynamics in 0.75PMN-0.25PT.

4.2.2 Local Cation Displacements. We examine cation-oxygen instantaneous PDF and time averaged PDF to investigate behavior of local dipole moments as a function of T through the phase transitions in 0.75PMN-0.25PT. Local cation off-centerings are obtained simply by subtracting the peak height positions of the PDFs from the high symmetry points in oxygen cages at the 0.75PMN-0.25PT lattice constants. In Figure 5, we show D_{inst}, the instantaneous local cation displacements, D_{static}, time-averaged static local cation displacements, and D_{dyn}, dynamic component defined as the difference between D_{inst} and D_{static}.

First, we discuss Pb local displacements in order to define local order parameters for the phase transitions in Figure 5a. It is clear that three phase transitions occur at $T_b = 550$ K, $T^* = 450$ K and $T_f = 375$ K. These values agree with experimental 0.75PMN-0.25PT data
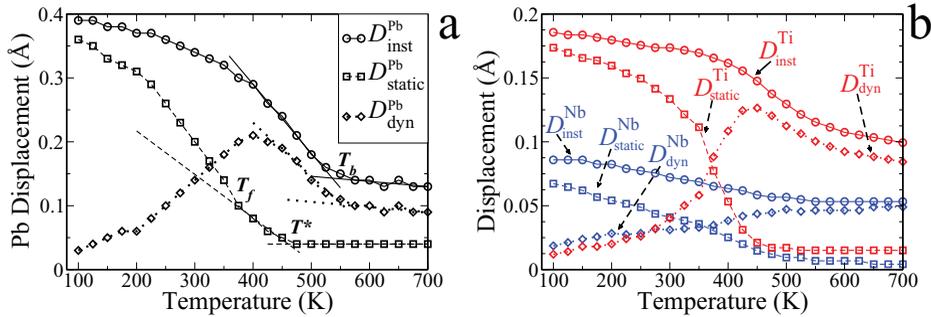
Figure 5. The magnitude of the instantaneous cation off-center displacement, D_{inst}, its static, D_{static}, and dynamic components, D_{dyn}, as a function of temperature. The D_{inst} and D_{static} for Pb atoms shown in (a) indicate the phase transitions at $T_b = 550$ K, $T^* = 450$, and $T_f = 375$ K. The Nb and Ti off-centerings in (b) follow almost the same trends in the Pb atom off-centering, but with a D_{dyn} peak at higher T. The data are taken from [23].

[32,33] and the temperatures which we estimated using the integrated $G(r, \omega)$ in Section IV B 1.. We note that D_{inst}^{Pb} shows that Pb atoms shift away from the center of the O_{12} by ≈ 0.15 Å and D_{static}^{Pb} reveals small Pb displacements even above T_b. The former is consistent with previous works [34–36] and the latter is due to the strong local random fields due to disorder in the *B*-cation arrangement [22,34]. However, the changes of the D_{inst}^{Pb} and D_{static}^{Pb} with temperature above 550 K are negligible, indicating that no phase transition takes place at high temperatures. For 550 K$>T>$400 K, D_{inst}^{Pb} rapidly increases with an equal slope.

The D_{inst}^{Pb} characterizes the transition from the paraelectric phase to the dynamic relaxor phase, something that has been lacking in the description of paraelectric-to-relaxor transition until now. On the other hand, D_{static}^{Pb} is still pinned at the value for $T > 550$ K and only starts slowly increasing below $T^* = 475$ K. The behavior of D_{Pb}^{static} obtained from the time averaged PDF is similar to the order parameter q obtained from the Edwards-Anderson spin glass model by means of the average magnitude of the static local polarization in PMN. [15,34] With the similarity to the q, thus, the transition at T^* can be characterized by the onset of the rise in D_{static}^{Pb}. A slow slope of D_{dyn}^{Pb} below 450 K implies that the dynamics change. The system transforms into the frozen phase at T=375 K as the D_{dyn}^{Pb} starts decreasing with slow increase in D_{inst}^{Pb} and rapid slope of D_{static}^{Pb}, and their subsequent saturation as T is lowered.

Inspection of the local cation displacements suggests that two approaches with the instantaneous and static local quantity are required to characterize the local order parameters in relaxors. The instantaneous information such as the D_{inst}^{Pb} provides the order parameter to describe the transition from the paraelectric phase to the dynamic relaxor phase. The order parameters for the lower temperature phases can be obtained from a static method such as previous investigations and the D_{static}^{Pb}.

4.2.3 Local Dynamics. To investigate the local correlations of the in-phase motions of Pb-Pb atomic pairs and Pb-*B*-cation pairs, we examine DPDF, $G(r, \omega)$ which provides the probability of vibrational frequencies at $g(r,t = 0)$ peak height positions for the atomic pairs. We consider the $G(r, \omega)$ Pb atomic pairs in neighboring cells along the $(n00)$, $(nn0)$ and (nnn) directions fto determine the extend of increased correlations predicted by the current PNR model. We find that enhancement of the correlations between Pb displacements
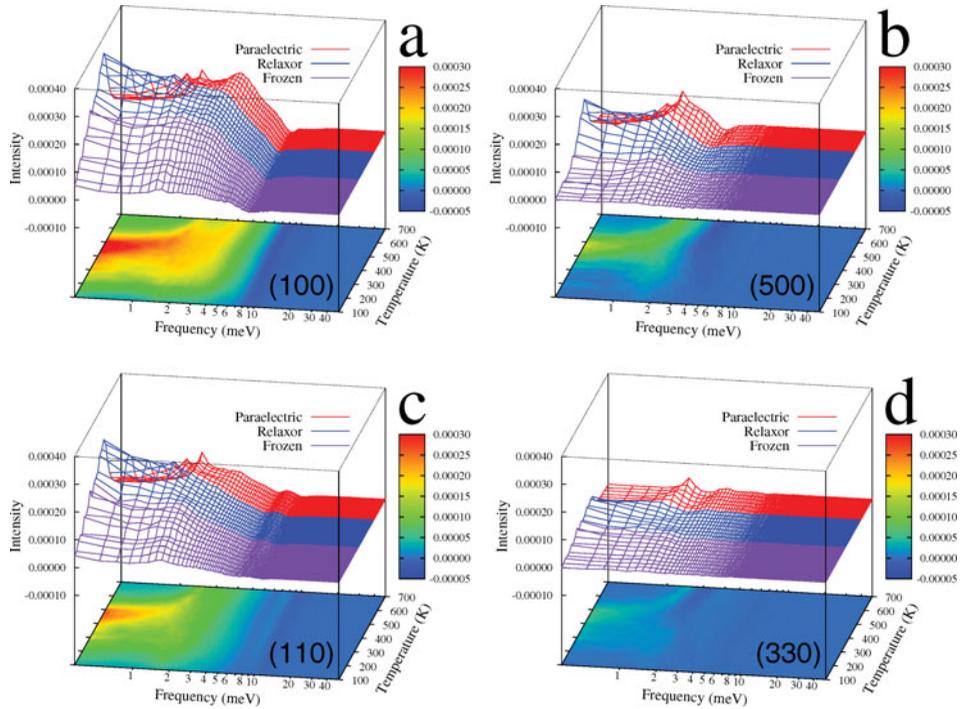
Figure 6. The Pb-Pb DPDF peaks represent in-phase vibrational motions of Pb pairs in cells for (a) (100), (b) (500), (c) (110), and (d) (330) directions as functions of T (K) and frequency (meV). The data are extracted from $G(r, \omega)$ at the peak position of the instantaneous PDF for each temperature. The color contour projected at bottom with a color bar shows the intensity of the peaks. For the Cartesian directions, enhanced intensity at low ω for $T < T_b$ is present even for large distances. For the non-Cartesian directions, low-frequency vibrations decay more rapidly with distance. The data are taken from [23].

between T_f and T_b strongly depends on direction. In Figure 6, we depict the Pb-Pb $G(r, \omega)$ along the (*n*00) and (*nn*0) directions; the intensities along (*nnn*) directions are only slightly weaker than the intensities along (*nn*0) directions.

Starting at T_b, the $G(r, \omega)$ along the (100) direction show a strong increase in intensity at low ω with a shift of the low frequency peak to below 0.1 meV on cooling. Below T^*, the $G(r, \omega)$ decreases in the low frequency region as T approaches T_f. Although the intensities are weaker for Pb atomic pairs separated by greater distances along the Cartesian directions, similar effects are apparent. However, along non-Cartesian directions, the $G(r, \omega)$ shows the strong changes only for the first neighbor cells. For larger distances, there is a rapid decrease of the Pb in-phase motion correlations at all temperatures (e.g. the (330) peak shown in Figure 6. This indicates that the local dipoles are strongly coupled along the Cartesian directions and between the nearest neighbors along non-Cartesian directions. The current PNR model cannot explain the strong anisotropy of the correlations since the correlations in the model should develop and extend along all directions.

The distinction between the Cartesian directions and other directions is more pronounced for Nb-Nb $G(r, \omega)$ in Figure 7, although there are no Nb-Nb pairs in the nearest neighbor cells along the Cartesian directions due to the random cite model for the *B*-site arrangement. The $G(r, \omega)$ intensities even for the fourth neighbor Nb-Nb along the
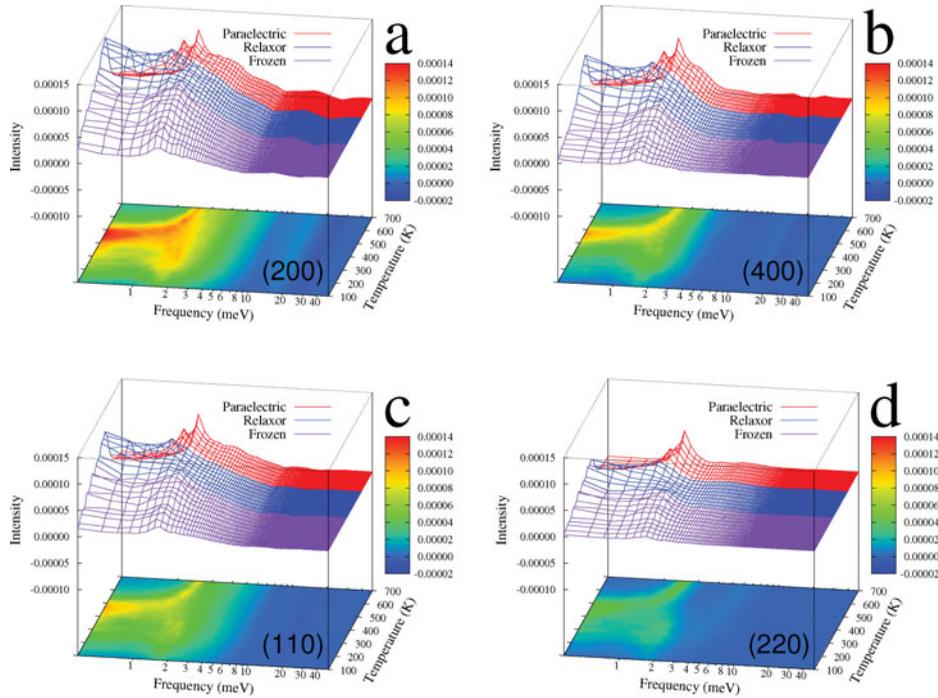
Figure 7. DPDF peaks for Nb-Nb pairs as functions of temperature (K) and frequency (meV) at *r* corrensponds to the peak position of the instantaneous PDF for each tempearture from [23]. with the projected color contour at bottom. A color bar shows the intensity of the peaks. The peaks of Nb atoms in the second neighbor cells along the Cartesian directions are shown in (a). (b) is the same as (a) but the fourth neighbor cells along the Cartesian directions. The Nb-Nb DPDFs between the first neighbors and the second neighbors along (110) directions are shown in (c) and (d), respectively. Direction rather than distance has a strong effect on the DPDF intensity.

Cartesian directions are higher than for the second neighbor Nb-Nb along the non-Cartesian directions. This contradicts the current PNR model since the peaks of the Nb-Nb $G(r, \omega)$ at shorter distances should be higher.

The anisotropic interactions are due to the through-oxygen interactions between nearest neighbor cations. Nearest neighbor Pb atoms share four oxygens along the (100) directions and one oxygen along the (110) directions (zero along the (111) directions). This makes the in-phase vibrations strongest along the (100) direction. Similarly, *B*-cation-*B*-cation interactions are mediated by oxygen atoms located along the Cartesian directions. As shown by the temperature dependence of DPDF intensity, the anisotropic correlations are absent for $T > T_b$ and their appearance at T_b is the characteristic feature of the paraelectric-to-relaxor phase transition. The strong, oxygen-mediated coupling between the dipoles observed in our simulation is similar to the hydrogen bond network in water. This network appears when super-heated water is cooled down and is transformed from a standard polar liquid structure dominated by dipole-dipole interactions into a directional H-bond network. Both relaxors and water exhibit unique structural and dynamic properties that are absent in other polar materials. Therefore, we suggest that the current PNR/matrix model should be replaced with that of a random network of anistotropically strongly coupled dipoles.

5. Conclusions

We have investigated the lead-based relaxors with density functional theory calculations and first principle based MD simulations. We have shown that the compositional relaxor-to-ferroelectric phase transitions can be predicted based on the local *B*-cation arrangement and the magnitude of the average *B*-cation displacement. Our MD simulations with with a nanoscale, 1080-atom supercell reproduced the experimental features of the dielectric response in PMN-PT and showed that slow dynamics in the relaxor phase are induced by the presence of the overbonded oxygen atoms. Together, these studies show that relaxor behavior can be obtained even in systems where due to the small simulations cell size there can be no coexisting PNR and matrix and that it is controlled by local structure features.

Finally, our local structure and dynamics investigations provide the characterization of the local order parameters and the anisotropic in-phase motion correlations which stem from oxygen-through coupling. The transition from dipole-dipole interactions to the coupling structurally through the under- and over-bonded oxygens anisotropically along the Cartesian directions at T_b resembles the changes from dipole-dipole interactions at high temperature to the coupling structurally through anisotropic hydrogen random network at room temperature in water. We therefore suggest that the random-network model is better suited for understanding relaxor behavior than the PNR/matrix model.

Funding

References

1. G. A. Smolenskii, V. A. Isupov, A. I. Agranovskaya, and S. N. Popov, *Sov. Phys. Solid State* **2**, 2584 (1961).
2. S.-E. Park and T. R. Shrout, *J. Appl. Phys.* **82**, 1804 (1997).
3. A. S. Mischenko, Q. Zhang, R. W. Whatmore, J. F. Scott, and N. D. Mathur, *Appl. Phys. Lett.* **89**, 242912 (2006).
4. Z. Kutnjak, J. Petzelt, R. and R. Blinc, *Nature* **441**, 956 (2006).
5. R. Blinc, V. Laguta, and B. Zalar, *Phys. Rev. Lett.* **91**, 247601 (2003).
6. J. F. Scott, *Science* **315**, 954 (2007).
7. P. M. Gehring, S.-E. Park, and G. Shirane, *Phys. Rev. Lett.* **84**, 5216 (2000).
8. G. Burns and F. H. Dacol, *Phys. Rev. B* **28**, 2527 (1983).
9. G. Burns and F. H. Dacol, *Solid State Commun.* **48**, 853 (1983).
10. D. Viehland, M. Wutting, and L. E. Cross, *Ferroelectrics.* **120**, 71 (1991).
11. L. E. Cross, *Ferroelectrics.* **76**, 241 (1987).
12. V. Westphal, W. Kleemann, and M. D. Glinchuk, *Phys. Rev. Lett.* **68**, 847 (1992).
13. H. D. Rosenfeld and T. Egami, *Ferroelectrics.* **150**, 183 (1993).
14. S. Vakhrushev, A. Nabereznov, S. K. Sinha, Y. P. Feng, and T. Egami, *J. Phys. Chem. Solids.* **57**, 1517 (1995).
15. R. Blinc, J. Dolinšek, A. Gregorovič, B. Zalar, C. Filipič, Z. Kutnjak, A. Levstik, and R. Pirc, *Phys. Rev. Lett.* **83**, 424 (1999).
16. R. Pirc and R. Blinc, *Phys. Rev. B.* **60**, 13470 (1999).
17. O. Svitelskiy, J. Toulouse, G. Young, and Z.-G. Ye, *Phys. Rev. B* **68**, 104107 (2003).
18. J. Toulouse, F. Jiang, O. Svitelskiy, W. Chen, and Z.-G. Ye, *Phys. Rev. B* **72**, 184106 (2005).

19. W. Dmowski, S. B. Vakhrushev, I.-K. Jeong, M. P. Hehlen, F. Trouw, and T. Egami, *Phys. Rev. Lett.* **100**, 137602 (2008).
20. P. M. Gehring, S.-E. Park, and G. Shirane, *Phys. Rev. B* **63**, 224109 (2001).
21. I. Grinberg, P. Juhás, P. K. Davies, and A. M. Rappe, *Phys. Rev. Lett.* **99**, 267603 (2007).
22. I. Grinberg, Y.-H. Shin and A. M. Rappe, *Phys. Rev. Lett.* **103**, 197601 (2009).
23. H. Takenaka, I. Grinberg, and A. M. Rappe, *Phys. Rev. Lett.* **110**, 147602 (2013).
24. N. Setter and L. E. Cross, *J. Appl. Phys.* **51**, 4356 (1980).
25. P. Juhás, P. K. Davies and M. A. Akbas, *J. Am. Ceram. Soc.* **87**, 2086 (2004).
26. B. P. Burton and E. Cockayne, *Phys. Rev. B* **60**, R12542 (1999).
27. I. Grinberg and A. M. Rappe, *Phys. Rev. B* **70**, 220101 (2004).
28. G. A. Samara, *Phys. Rev. Lett* **77**, 314 (1996).
29. R. E. Cohen, *Nature* **358**, 136 (1992).
30. P. K. Davies and M. A. Akbas, *J. Phys. Chem. Solids* **61**, 159 (2000).
31. Online supplementary material at http://journals.aps.org/prl/abstract/10.1103/PhysRevLett.110.147602#supplemental.
32. B. Dkhil, P. Gemeiner, A. Al-Barakaty, L. Bellaiche, E. Dul'kin, E. Mojaev, and M. Roth, *Phys. Rev. B* **80**, 064103 (2009).
33. A. A. Bokov and Z. -G. Ye, *Appl. Phys. Lett.* **77**, 1888 (2000).
34. M. Sepliarsky and R. E. Cohen, *J. Phys. Condens. Matter* **23**, 435902 (2011).
35. Y. -H. Shin, V. R. Cooper, I. Grinberg, and A. M. Rappe, *Phys. Rev. B* **71**, 054104 (2005).
36. M. Paściak, T. R. Welberry, J. Kulda, M. Kempa, and J. Hlinka, *Phys. Rev. B* **85**, 224109 (2012).